Electronic Supplementary Material (ESI) for Catalysis Science & Technology.

Selective CO_2 methanation on Ru/TiO_2 catalysts: unravelling the decisive role of the TiO_2 support crystal structure

A. Kim,[a,b] C. Sanchez,[b] G. Patriarche,[c] O. Ersen,[d] S. Moldovan,[d] A. Wisnet,[e] C. Sassoye,*[b] D. P. Debecker*[a]

[a.] *Institute of Condensed Matter and Nanoscience - MOlecules, Solids and reactiviTy (IMCN / MOST).Université catholique de Louvain. Croix du Sud 2 box L7.05.17, 1348 Louvain-La-Neuve, Belgium*

[b.] *Sorbonne Universités, UPMC Univ Paris 06, CNRS, Collège de France, Laboratoire de Chimie de la Matière Condensée de Paris, 11 place Marcelin Berthelot, 75005 Paris, France*

[c.] *Laboratoire de Photonique et de Nanostructures (LPN), CNRS, UniversitÃ© Paris-Saclay, route de Nozay, F-91460 Marcoussis, France*

[d.] *Institut de Physique et Chimie des Matériaux de Strasbourg, UMR7504 CNRS-UNISTRA and NIE, 23 rue du Loess, B.P. 43, 67034 Strasbourg cedex 2, France*

[e.] *Department of Chemistry and CeNS, Ludwig-Maximilians-University, Butenandtstrasse 11, 81377 Munich, Germany*

† Footnotes relating to the title and/or authors should appear here.

Supporting Information

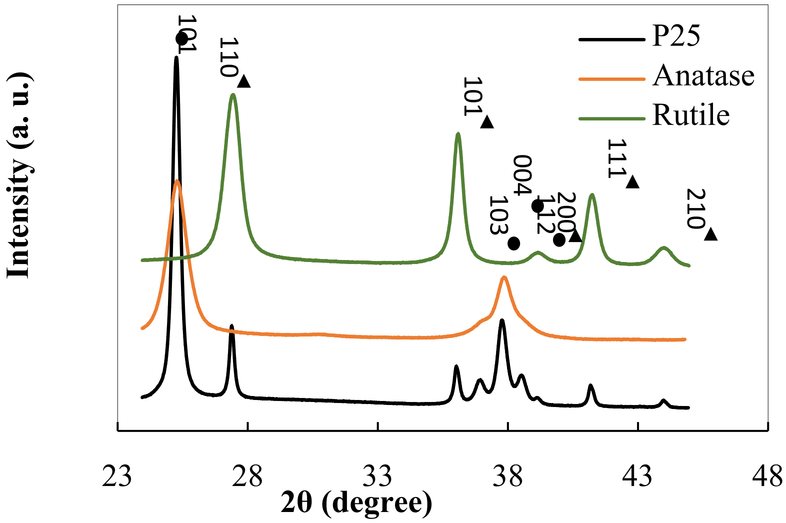

SI-1. XRD patterns of the support prior RuO_2 deposition. P25 TiO_2 (anatase (❧) and rutile(①)) in black; anatase TiO_2 in orange and rutile TiO_2 in green.

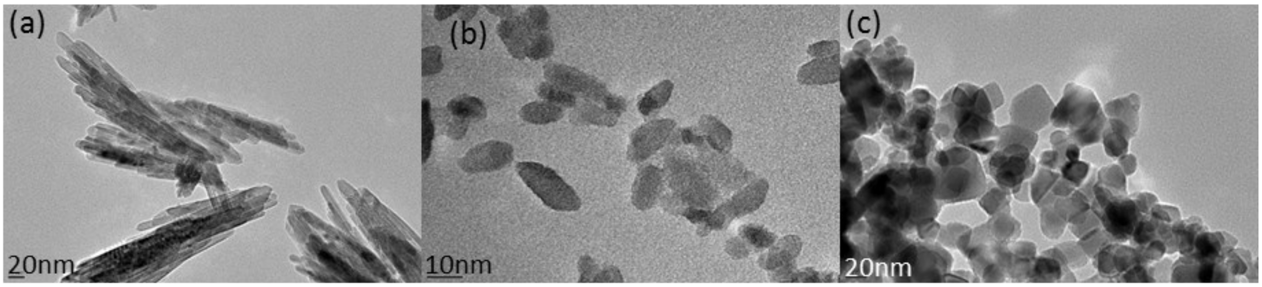

SI-2: TEM images showing the morphology of the TiO_2 support particle alone, prior RuO_2 deposition. (a) rutile, (b) anatase and (c) P25.

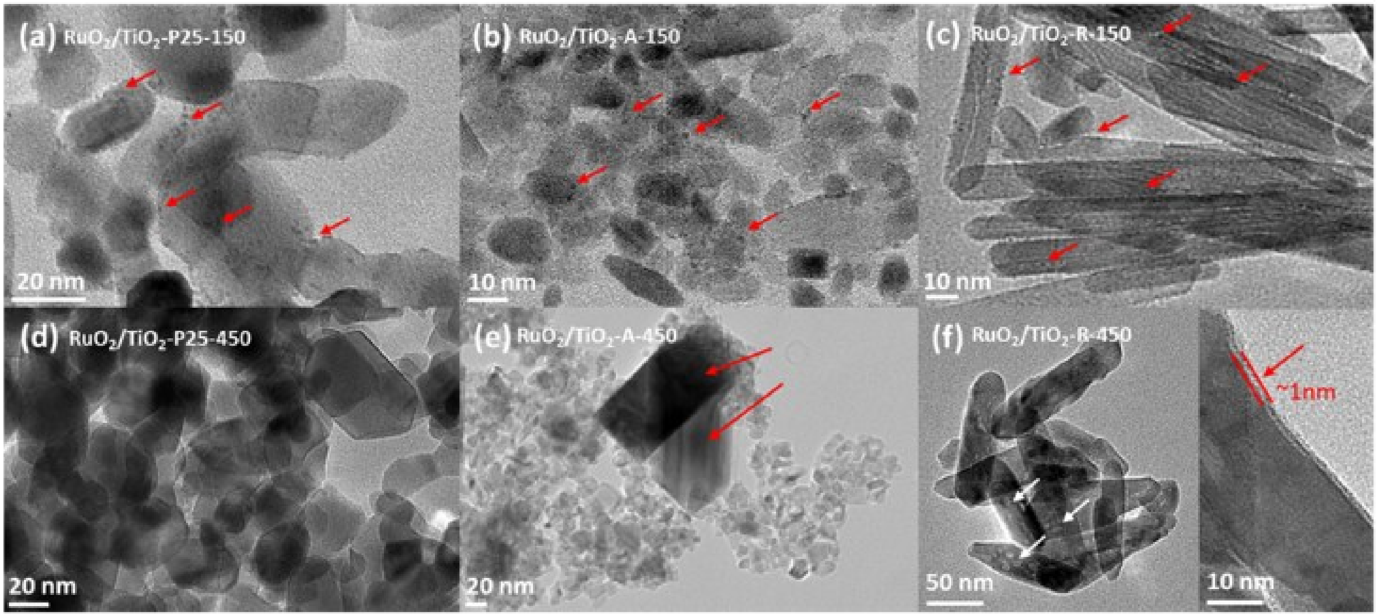

SI-3. TEM micrographs of RuO_2/TiO_2 catalysts annealed at 150 °C; (a) on P25, (b) on anatase , and (c) on rutile, and TEM micrograph of the same catalysts after being annealed at 450 °C; (d) on P25, (e) on anatase, and (f) on rutile TiO_2, respectively. Red arrows point RuO_2 and white arrows point RuO_2- depleted areas.

SI-4. TEM tomography (3D analysis) that underlines the quite uniform distribution of RuO_2 NPs on P25 TiO_2 nanoparticles after annealing at 150 °C. Media file corresponding to the tomography analysis: **initial-mix.avi**

	Ru (w%)
RuO2/TiO2-P25-450	2,43
RuO2/TiO2-A-450	2,35
RuO2/TiO2-R-450	2,60

SI-5: ICP-AES elemental analysis of the 450°C annealed catalyst. Small variations in the Ru content come from water variation content in the $RuCl_3.xH_2O$ (x= 3-5) precursor.

Annealing Temperature (°C)	Reaction Temperature (°C)	CH_4 production rate ($\mu mol_{CH4}\ g_{cat}^{-1}\ s^{-1}$)		
		RuO_2/TiO_2-P25	RuO_2/TiO_2-A	RuO_2/TiO_2-R
150	50	0.000	0.000	0.000
	85	0.000	0.000	0.000
	100	0.000	0.000	0.000
	125	0.000	0.005	0.000
	150	0.016	0.023	0.013
	165	0.035	0.050	0.033
	185	0.076	0.109	0.082
	200	0.126	0.167	0.145
250	50	0.000	0.001	0.000
	85	0.005	0.006	0.000
	100	0.017	0.019	0.006
	125	0.069	0.075	0.030
	150	0.184	0.208	0.099
	165	0.317	0.395	0.185
	185	0.583	0.745	0.402
	200	0.848	1.025	0.619
350	50	0.000	0.001	0.000
	85	0.012	0.008	0.000
	100	0.032	0.021	0.008
	125	0.113	0.084	0.050
	150	0.316	0.256	0.155
	165	0.543	0.447	0.287
	185	1.014	0.919	0.562
	200	1.464	1.310	0.903
450	50	0.000	0.000	0.000
	85	0.018	0.010	0.004
	100	0.045	0.027	0.012
	125	0.160	0.102	0.047
	150	0.435	0.282	0.143
	165	0.898	0.532	0.283
	185	1.707	1.048	0.602
	200	2.572	1.588	0.982
550	50	0.000	0.000	0.000
	85	0.013	0.006	0.000
	100	0.035	0.017	0.006
	125	0.125	0.070	0.026
	150	0.362	0.205	0.092
	165	0.713	0.350	0.178
	185	1.436	0.594	0.419
	200	2.202	0.952	0.656

SI-6. Catalytic activities of different TiO_2 supported catalysts at various annealing temperatures and reaction temperatures

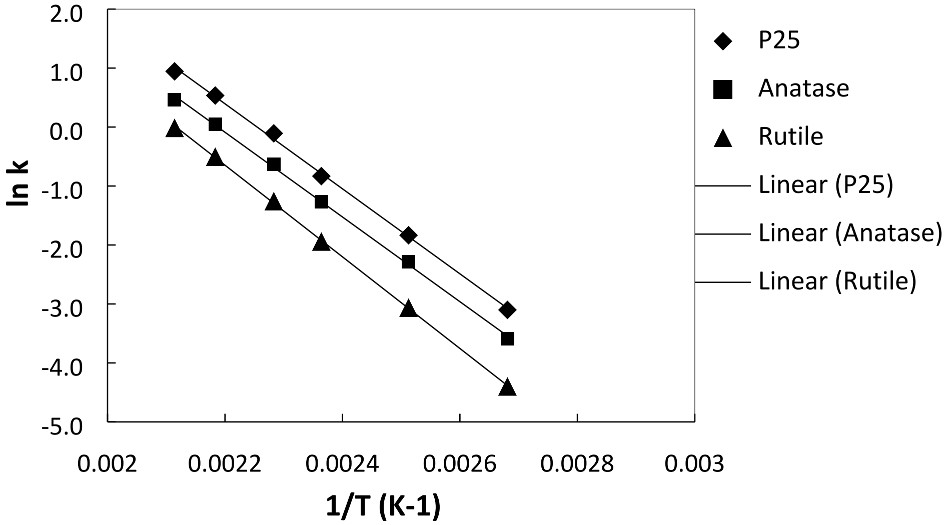

SI-7. Arrhenius plot for determination of activation energy obtained from 100 to 200 °C reaction temperatures.

Annealing T (°C)	**P25**	**Anatase**	**Rutile**	
			width	**length**
150	28	6	11	100
250	22	8	11	105
350	25	10	17	95
450	25	11	24	97

SI-8: TiO_2 particle size (in nm) of RuO_2/TiO_2 catalysts measured by TEM analysis

		rutile			anatase				mean size (Å)
	(°C)	**110**	**101**	**200**	**101**	**103**	**004**	**112**	
P25	**150**	48	49	55	27	25	23	24	36
	250	53	51	39	27	26	23	24	35
	350	49	48	34	27	25	23	24	33
	450	52	48	32	27	27	23	25	33
anatase	**150**				10	10	13	8	10
	250				10	10	14	8	10
	350				11	16	13	8	12
	450				16	17	17	15	16,0
rutile	**150**	12		13					13
	250	13		14					14
	350	16		17					17
	450	21		20					21

SI-9. TiO_2 support particle sizes calculated from the Scherrer equation. In case of pure rutile TiO_2 support, only the widths of the needle are calculated.

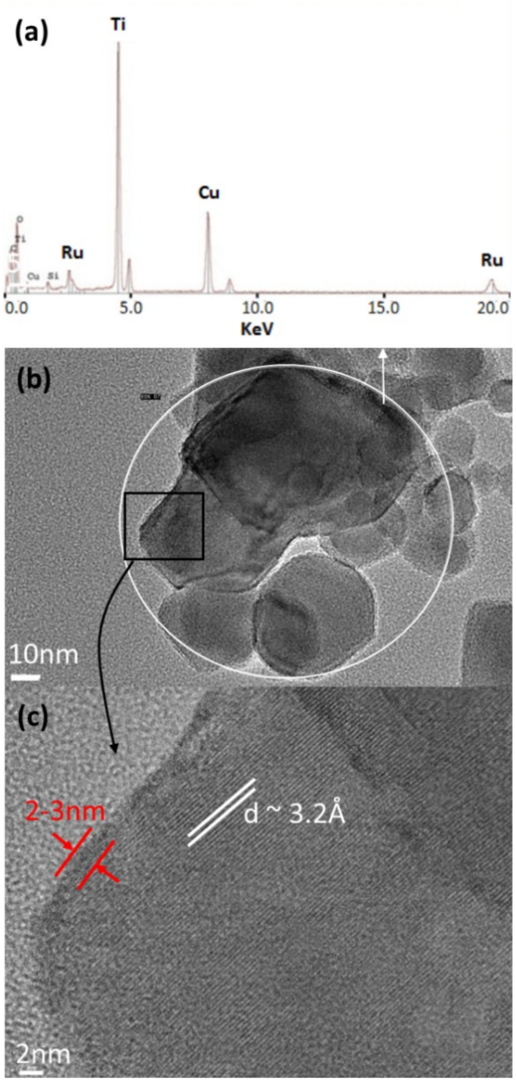

SI-10. RuO_2/TiO_2-P25-250. (a) EDX spectrum showing the presence of Ru; (b) TEM images showing the presence of Ru on rutile TiO_2 particles and the EDX analysis; (c) zoomed image of a catalyst particle corresponding to the d-spacing of rutile phase. Red arrows indicate the thickness of RuO_2 aggregates/layers.

		hkl	P25 support		anatase support		rutile support	
			2θ (°)	**FWHM (°)**	**2θ (°)**	**FWHM (°)**	**2θ (°)**	**FWHM (°)**
150°C	**anatase**	101	25,2946	0,3419	25,2544	0,8953		
	TiO_2 rutile	110	27,4262	0,2105			27,4015	0,7226
	RuO_2	110						
	RuO_2	101						
	TiO_2 rutile	101	36,0699	0,2082			36,0602	0,4556
	anatase	103	36,9544	0,3691	36,9435	0,9111		
	anatase	004	37,8196	0,3959	37,8177	0,6631		
	anatase	112	38,5640	0,3801	38,5289	1,0937		
	TiO_2 rutile	200	39,1837	0,1927			39,2081	0,6722
250°C	**anatase**	101	25,3095	0,3412	25,2761	0,8814		
	TiO_2 rutile	110	27,4552	0,1924			27,4104	0,6663
	RuO_2	110						
	RuO_2	101	-	-				
	TiO_2 rutile	101	36,0550	0,2016			36,0518	0,4407
	anatase	103	36,9715	0,3597	37,0052	0,8381		
	anatase	004	37,8274	0,4018	37,8564	0,6431		
	anatase	112	38,5701	0,3869	38,5308	1,0354		
	TiO_2 rutile	200	39,2214	0,2512			39,1536	0,6193
350°C	**anatase**	101	25,3147	0,3424	25,2918	0,7784		
	TiO_2 rutile	110	27,4642	0,2040			27,4084	0,5366
	RuO_2	110	27,7428	0,6486	27,9673	1,0202		
	RuO_2	101	35,3337	1,2289	35,0446	0,5075		
	TiO_2 rutile	101	36,0624	0,2109			36,0466	0,3822
	anatase	103	36,9731	0,3664	36,9923	0,5518		
	anatase	004	37,8292	0,4031	37,8831	0,6769		
	anatase	112	38,5728	0,3839	38,5370	1,1692		
	TiO_2 rutile	200	39,2401	0,2883			39,1527	0,5385
450°C	**anatase**	101	25,3259	0,3345	25,2678	0,5608		
	TiO_2 rutile	110	27,4777	0,1970	27.5107	0.4342	27,4084	0,4332
	RuO_2	110	27,7222	0,5689	27,9774	0,4925		
	RuO_2	101	35,4020	1,1626	35,0278	0,5013		
	TiO_2 rutile	101	36,0676	0,2128	35.7809	0.7159	36,0495	0,3158
	anatase	103	36,9830	0,3520	36,9656	0,5313		
	anatase	004	37,8387	0,3930	37,8282	0,5451		
	anatase	112	38,5826	0,3726	38,5464	0,5902		
	TiO_2 rutile	200	39,2594	0,2974			39,1617	0,4659

SI-11. Deconvolution of XRD peaks from 150 to 450 °C on the various support (P25, anatase and rutile). RuO_2 peaks can only be deconvoluted with reasonable width from high temperature on P25 and anatase. The proximity of the RuO_2 peaks to TiO_2 rutile prevents deconvolution of RuO_2 peak on the pure rutile TiO_2 support.

The difference in cell parameters cannot be linked only with Ti^{4+} and Ru^{4+} radii (0.605 Å and 0.620 Å respectively; a(RuO_2) is smaller than a(TiO_2) and c(RuO_2) is bigger than c(TiO_2).[1] Accordingly, d_{110} (RuO_2) (3.183 Å) is smaller than d_{110} (TiO_2) (3.247 Å), and d_{101} (RuO_2) (2.558 Å) is bigger than d_{101} (TiO_2) (2.487 Å).

The rutile structure can be briefly described as distorted MO_6 octahedra connected by their edges to form chains along the [001] direction. These chains are linked together by the octahedra vertices in the directions [110] and [1-1 0] .

The consequence of differences in cell parameters is that the slightly distorted MO_6 octahedral are not oriented in the same way for RuO2 and TiO2 rutile structures: Two short Ru-O bonds (1.942 Å) propagate along the [110] direction for RuO_2 whereas this direction concerns the two long Ti-O bonds (1.978Å) for TiO_2. For RuO_2, the four remaining long Ru-O bonds (1.984 Å) are strongly governed by the c axis, whereas in case of TiO_2, the four short Ti-O bonds (1.945 Å) are restricted by the c axis. Accordingly, the significant increase of d_{110} (RuO_2) upon RuO_2 crystallization in proximity to rutile TiO_2 means an increase in length of the two short Ru-O bonds. Similarly, the decrease of d_{101} (RuO_2) contributes mostly to the decrease in the length of the long Ru-O bonds. Thus, in RuO_2/TiO_2-P25 catalyst, the shifts in the (110) and (101) RuO_2 peak positions respectively towards the (110) and (101) rutile TiO_2 peaks indicate that RuO_2 nanoparticles are apt to crystallize adopting the rutile TiO_2 structure, which is referred to as epitaxial growth. This means that RuO_6 octahedral is globally less distorted in presence of rutile phase of P25 support than being crystallized into RuO_2 structure alone.

SI-12. Explanation on the shift in RuO_2 peak positions towards rutile TiO_2 peak positions and its consequences on the RuO_2 structure.

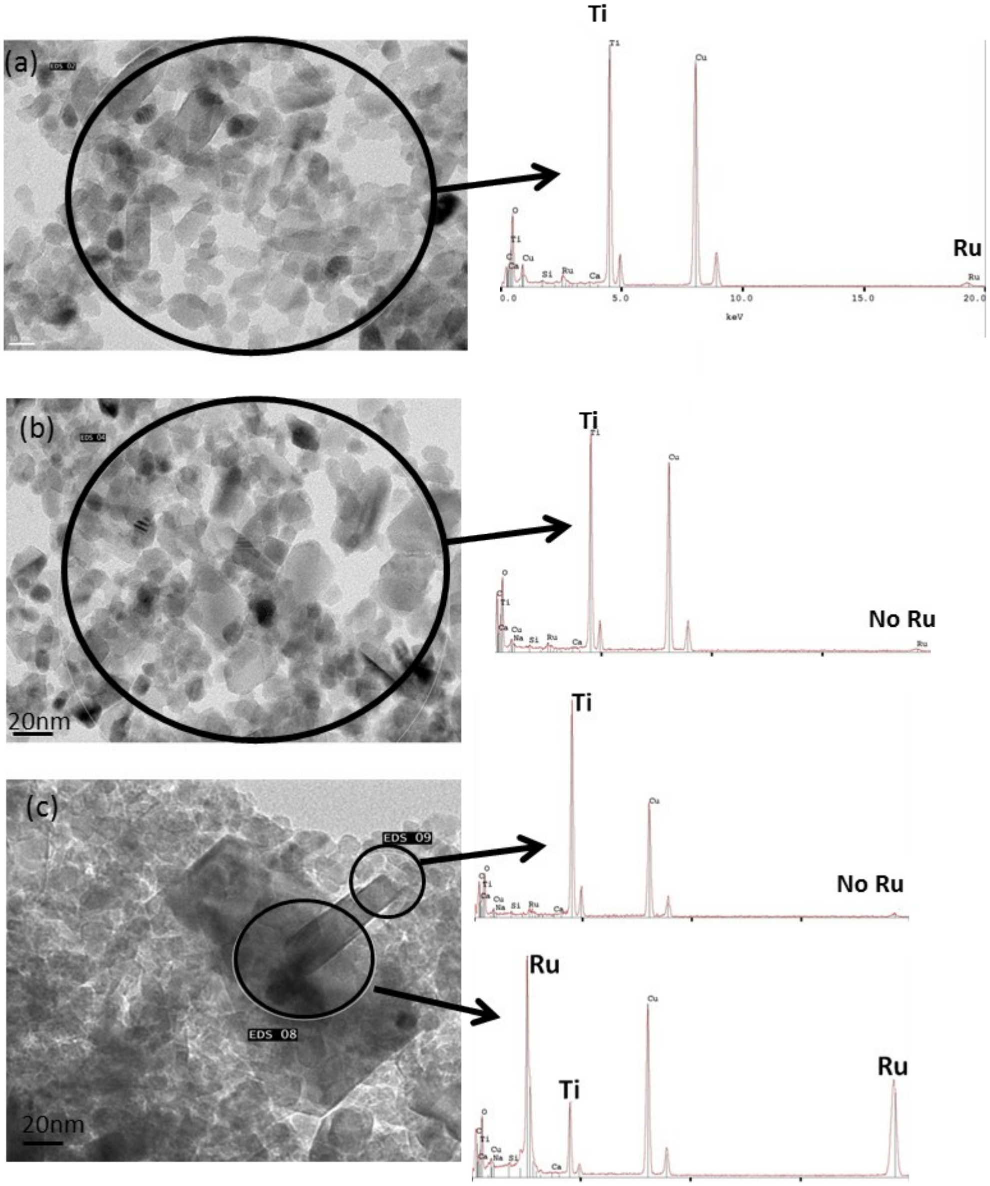

SI-13: TEM images of RuO_2/TiO_2-A catalyst annealed at 250°C (a) and 350°C (b-c) with the corresponding EDX analysis showing a good dispersion of RuO_2 at 250°C, and RuO_2 big crystals (c) separated from TiO_2 naked anatase (b) on which rutile TiO_2 has grown (c) at 350°C.

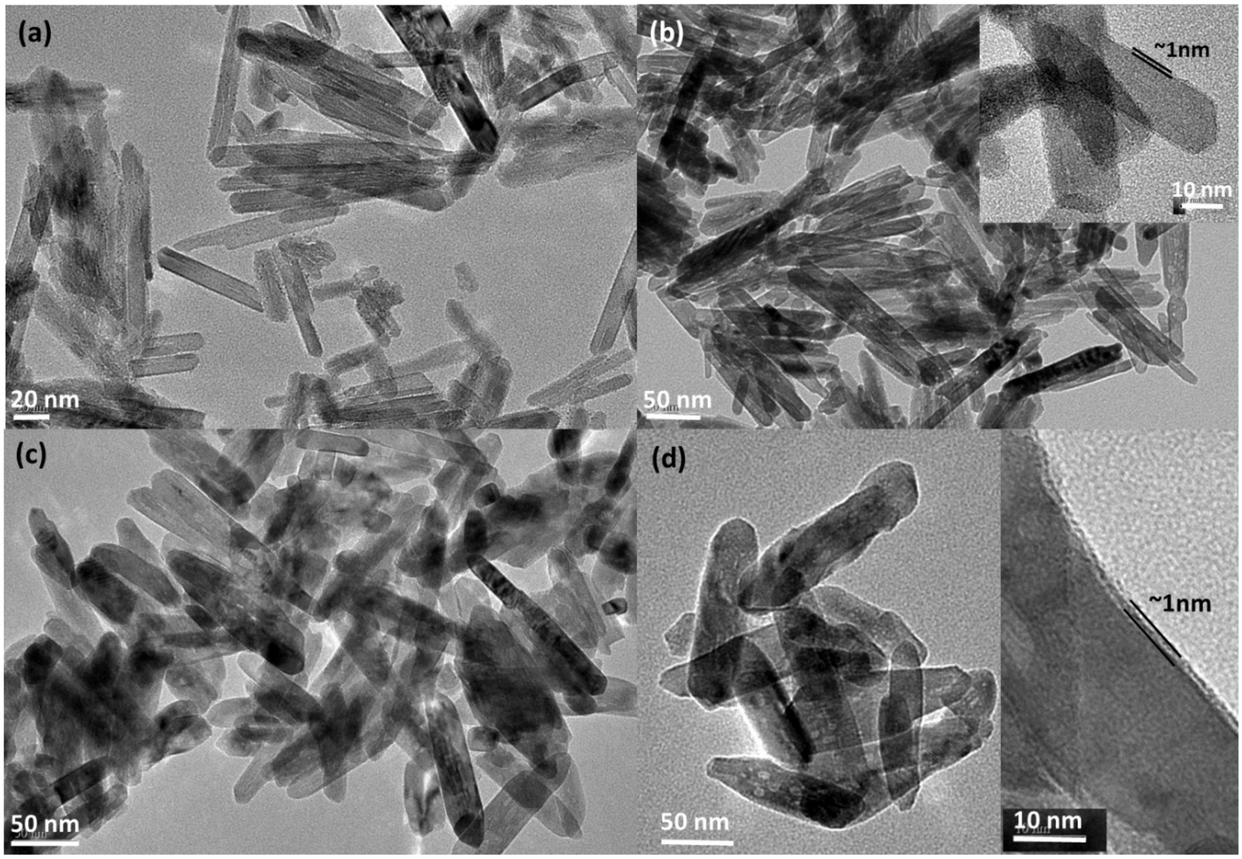

S-14. TEM images of RuO_2/TiO_2-R after annealing at (a) 150°C, (b) 250 °C, (c) 350 °C, and (d) 450 °C.

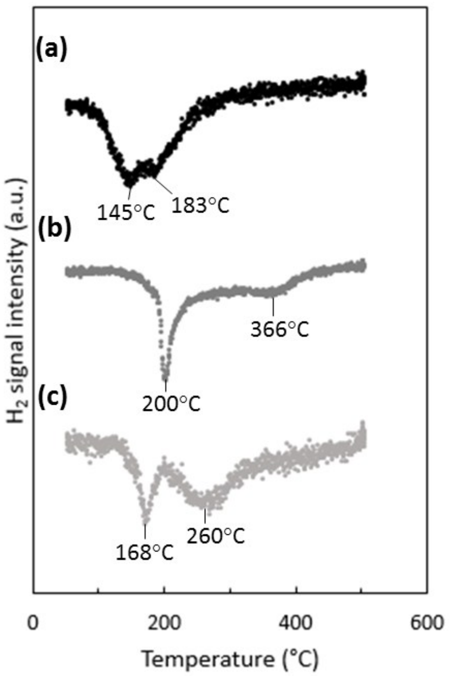

SI-15: TPR results for (a) RuO_2/TiO_2-P25-450, (b) RuO_2/TiO_2-A-450, and (c) RuO_2/TiO_2-R-450.

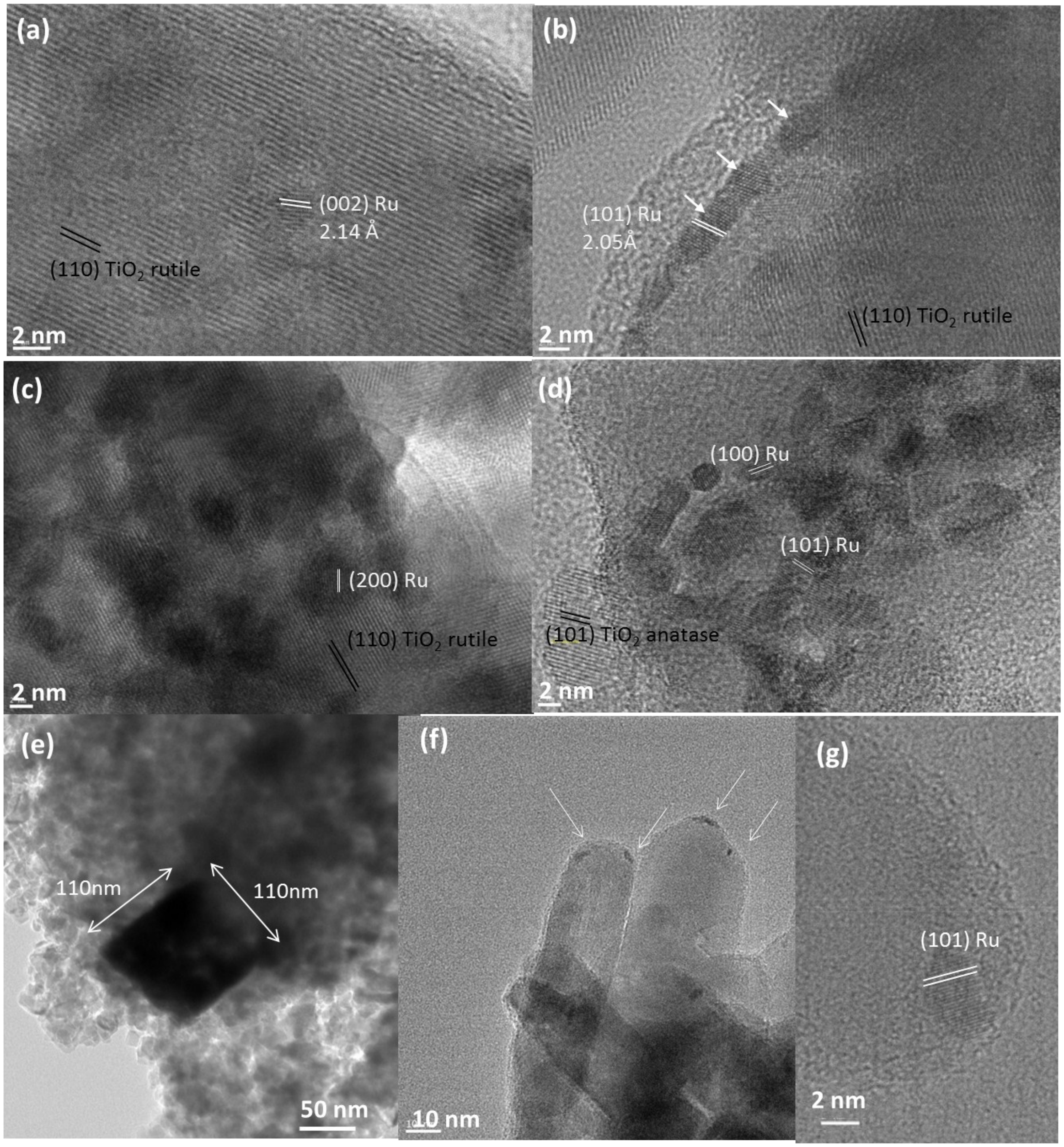

SI-16: HR-TEM pictures of the 450°C-catalysts post methanation clearly showing the Ru crystallographic planes on all support: Rutile TiO_2 from P25 support (a-b), anatase TiO_2 support (c-e) and rutile TiO_2 support (f-g). On anatase support, few TiO_2 rutile planes are distinguished, coming from RuO_2 -promoted crystallization (c); few compact Ru aggregate, too thick to allow the electron beam to fully distinguish the Ru particles present the global shapes and sizes of RuO_2 crystals prior reduction (e).

SI-17. TEM tomography (3D analysis) of the P¨25-450 tested catalyst that underlines the presence of Ru patches only on specific TiO2 P25 particles. Media file corresponding to the tomography analysis :**test-mix.avi**

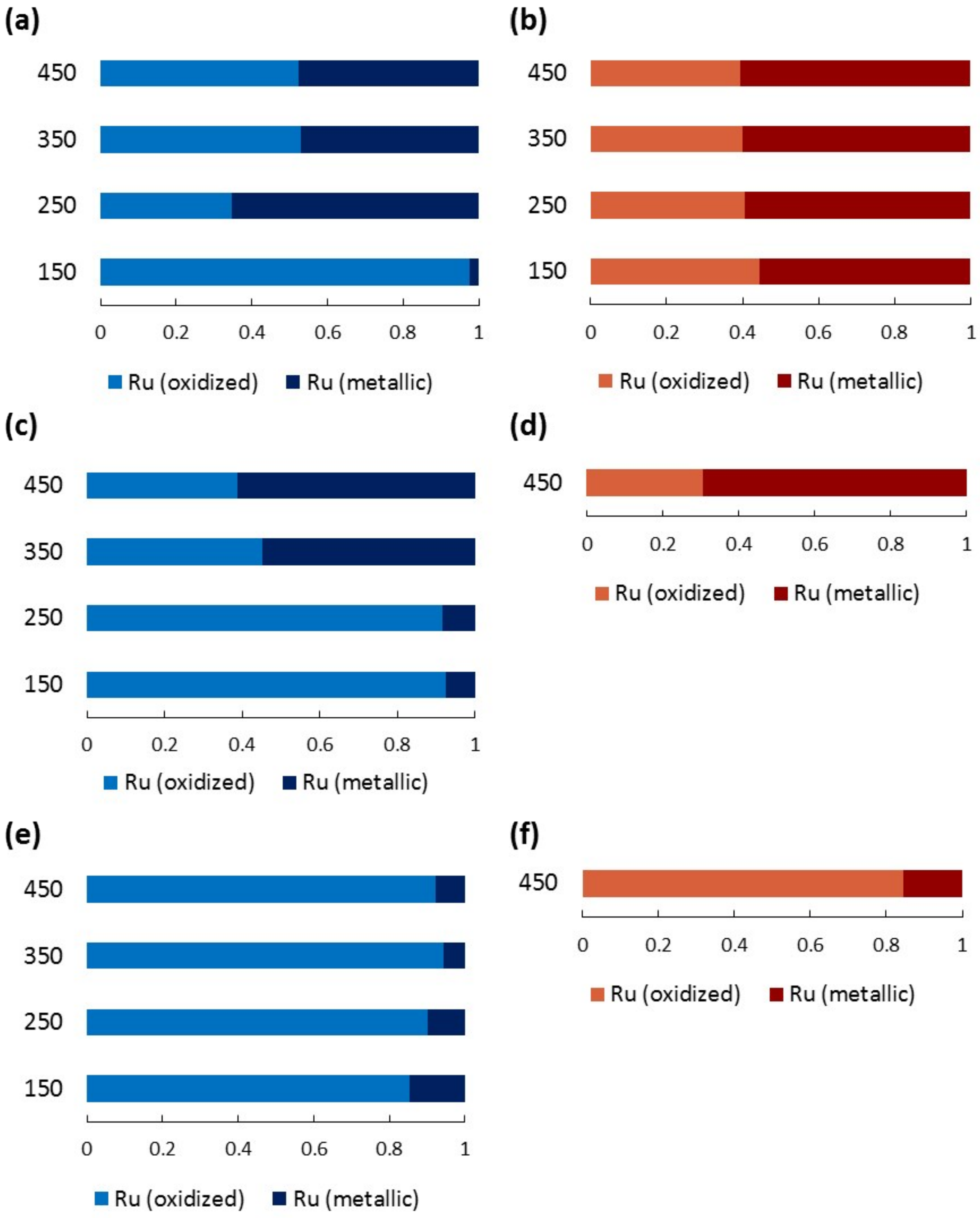

SI-18. Proportions of oxidized and metallic Ru species by XPS; (a) RuO_2/TiO_2-P25 (before reduction), (b) Ru/TiO_2-P25 (after methanation), (c) RuO_2/TiO_2-A (before reduction), (d) Ru/TiO_2-A (after methanation), (e) RuO_2/TiO_2-R (before reduction), and (f) Ru/TiO_2-R (after methanation)

The Scherrer equation was used to calculate the crystallite size of particles:

$$s = \frac{K.\lambda}{\beta cos\theta}$$

s = mean size perpendicular to hkl plane (Å)

K the shape factor, 0.9 for this study

λ = the XRay wavelength (1.5419Å, the mean wavelength for Kα1 Kα2 ray)

β = the peak broadening at half maximum intensity in radian, taking into account 0.04° broadening in the used 2θ range for the instrument.

From TEM analysis, P25 particles and pure anatase shows roughly isotropic shapes whereas pure rutile TiO_2 particle crystalize as c-axis oriented needles. Thus, TiO_2 particle sizes were calculated using Scherrer equation from rutile (110), (101), (200) peaks and anatase (101), (103), (004) and (112) peaks for both P25 and pure anatase support. With the (001) rutile diffraction peak being forbidden, no easy estimation of the rutile needle length could be made. However, rutile needle width could be estimated from the (110) and (200) diffraction peaks; (101) and (111) diffraction peaks were excluded for this calculation because of their combined a- and c-axes influence.

S-19. Procedure of evaluating TiO_2 crystal size using Scherrer equation.

The redistribution process of RuO_2 during heat treatment from anatase TiO_2 particles to rutile TiO_2 particles appears to play a major role into the catalyst activation. As previously observed by Xiang et al.[2], this phenomenon only occur for small RuO_2 particles (2 nm or smaller). In this size range, it is well known that surface tension dominates most physicochemical properties of nanomaterials, especially the interface behaviour and surface stability. When thermal energy (heat) is applied to the system, the small RuO_2 particles can overcome the constraints from the bulk network in order to minimize global free energy, either by diffusion to grow into bigger particles or undergoing shape change. The shape transformation (from sphere to thin layer) is driven by the surface relaxation due to epitaxy stabilization at the interface of rutile TiO_2 and RuO_2. The mechanism of departure of the ruthenium atoms from anatase TiO_2 surface remains less clear. Two possible pathways can be proposed: RuO_2 local volatilization followed by redeposition and RuO_2 nanoparticle diffusion.

Indeed, RuO_2 vaporization/condensation phenomena have been addressed in the fabrication of α-Al_2O_3 at 1000 °C with RuO_2 crystals trapped in the matrix, presenting a Ru gradient from the core of the sample to the surface.[3] Upon heating in oxidative atmosphere, the two following equilibrium can be considered:

$$RuO_2\ (s) + O_2 = RuO_4\ (g) \qquad (1)$$

$$RuO_2\ (s) + \tfrac{1}{2}\, O_2 = RuO_3\ (g) \qquad (2)$$

In this way, during heat activation, RuO_2(s) on TiO_2 support could be locally vaporized as RuO_x gas and randomly redeposited as RuO_2 on other TiO_2 surface. When deposited on rutile TiO_2, stabilization and fixation would occur through epitaxy. Vaporization would occur again for RuO_2 on anatase support, until RuO_2 could be redeposited on rutile TiO_2.

However, the amount of RuO_x gas in equilibrium with RuO_2 usually remains very low: For example, under pure oxygen static atmosphere (1 atm), vapour pressure has been measured at 0,2. 10^{-3} atm at 1000 °C.[4,5] Thermodynamic calculations, based on experiments, have allowed to establish the total RuO_x vapour pressure depending on the atmosphere and temperature: [6]

$$P(RuO_4)=\exp(20.002 - 2.2867*\ln T - 15562.5/T + \ln P(O_2))$$

$$P(RuO_3)=\exp(37.939 - 3.0590*\ln T - 32488.1/T + 0.5*\mathrm{Ln}P(O_2))$$

Given these equations, the RuO_x vapour pressure reaches 1.2. 10^{-8} atm only at 450°C in air. According to Le Chatelier's principle, both equilibrium can be displaced: towards volatilization under high oxygen gas flow, or towards RuO_2 deposition from RuO_3/RuO_4 rich atmosphere.[7] This explain why the rare studies published concerning pure bulk (unsupported and unstabilised) RuO_2 catalyst in automotive for NO_x reduction report that, under extremely high gas flow (100000 h^{-1} space velocity), a drastic loss of ruthenium occurs over time.[8] Of course, our static conditions of heat treatment at 450 °C in static air do not favour this volatilization of RuO_4 and RuO_3. Here, the Ru initial loading is preserved during our entire process (from RuO_2 deposition until the end of the catalytic test). Thus, if volatilization cannot be thermodynamiquelly totally excluded, it has to remain un-favoured, local (volatilization followed by immediate redeposition) and partial under our experimental conditions.

Small RuO_2 nanoparticles, on the other hand, have already been proven to be able to diffuse at the surface of particles. Indeed, at temperature as low as 300 °C, small RuO_2 nanoparticles embedded into amorphous silica matrix can diffuse and grow at the surface of the RuO_2/SiO_2 composite layer in the generated porosity path, whereas larger RuO_2 particles (above 4nm) lose their ability to diffuse and remain trapped.[9]

The driving force of this diffusive sintering phenomenon can be understood in terms of two operative mechanisms: Ostwald ripening (OR) or particle migration and coalescence (PMC). OR involves interparticle transport of mobile molecular species (clusters), driven by differences in free energy and local adatom concentrations on the support surface. In contrast, PMC involves the mobility of particles in a Brownian-like motion on the support surface, with subsequent coalescence when particles come in close proximity to each other. In the early stage of diffusive sintering, evidence from recent in situ studies suggest that OR dominates the diffusion of nanoparticles towards sintering when particles are very small.[10–13]

In this current study, the diffusion driven by OR explains the migration of RuO_2 nanoparticles at the surface of TiO_2 particle. Subsequently, the diffusion of RuO_2 nanoparticles leads to two different phenomena in terms of sintering: isotropic growth of RuO_2 crystals on pure anatase TiO_2 and epitaxial growth of RuO_2 layers on rutile TiO_2 (P25 and pure TiO_2 rutile support)

SI-20. RuO_2 nanoparticles migration discussion

References

1 R. D. Shannon, *Acta Crystallogr., Sect. A*, 1976, **A32**, 751–767.

2 G. Xiang, X. Shi, Y. Wu, J. Zhuang and X. Wang, *Sci. Rep.*, 2012, **2**, 801.

3 L. Ji, J. Lin and H. C. Zeng, *Chem. Mater.*, 2001, **13**, 2403–2412.

4 W. E. Bell and M. Tagami, *J. Phys. Chem.*, 1963, **67**, 2432–2436.

5 H. Schaefer, A. Tebben, W. Gerhardt, V. Harald and A. Tebben, *Z. Anorg. Allg. Chem.*, 1963, **321**, 41–55.

6 F. Garisto, *AECL-9552, Whiteshell Nucl. Res. Establ.*, 1988.

7 M. T. Colomer and M. J. Velasco, *J. Eur. Ceram. Soc.*, 2007, **27**, 2369–2376.

8 H. S. Gandhi, H. K. Stepien and M. Shelef, *Mater. Res. Bull.*, 1975, **10**, 837–845.

9 X. Paquez, G. Amiard, G. de Combarieu, C. Boissiere and D. Grosso, *Chem. Mater.*, 2015, **27**, 2711–2717.

10 T. W. Hansen, A. T. De La Riva, S. R. Challa, A. K. Datye, A. T. Delariva, S. R. Challa and A. K. Datye, *Acc. Chem. Res.*, 2013, **46**, 1720–1730.

11 S. B. Simonsen, I. Chorkendorff, S. Dahl, M. Skoglundh, J. Sehested and S. Helveg, *J. Am. Chem. Soc.*, 2010, **132**, 7968–7975.

12 K. Yoshida, A. Bright and N. Tanaka, *J. Electron Microsc.*, 2012, **61**, 99–103.

13 A. D. Benavidez, L. Kovarik, A. Genc, N. Agrawal, E. M. Larsson, T. W. Hansen, A. M. Karim and A. K. Datye, *ACS Catal.*, 2012, **2**, 2349–2356.